Supplementary Information

Controlling the gate-sorption properties of solid solutions of Werner complexes by varying component ratios

Shin-ichiro Noro,*[ab] Yu Song,[b] Yutaro Tanimoto,[b] Yuh Hijikata,[c] Kazuya Kubo,[d] and Takayoshi Nakamura*[e]

[a] Faculty of Environmental Earth Science, Hokkaido University, Sapporo 060-0810, Japan.
[b] Graduate School of Environmental Science, Hokkaido University, Sapporo 060-0810, Japan.
[c] Institute for Chemical Reaction Design and Discovery (WPI-ICReDD), Hokkaido University, Sapporo, 001-0021, Japan
[d] Graduate School of Material Science, University of Hyogo, 3-2-1 Kouto, Kamigori-cho, Ako-gun, Hyogo 678-1297, Japan
[e] Research Institute for Electronic Science, Hokkaido University, Sapporo 010-0020, Japan

Table of contents

1. ATR-IR spectra

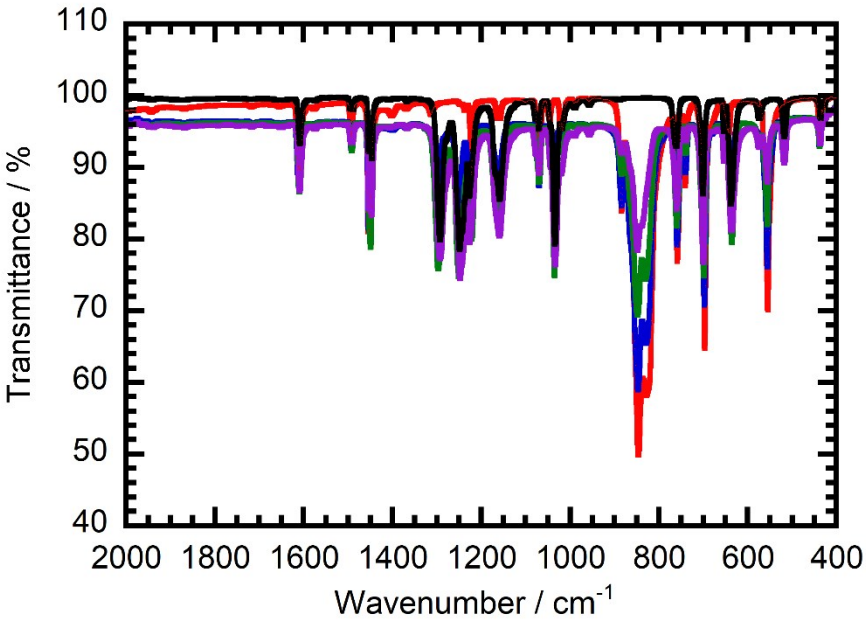

Fig. S1. ATR-IR spectra of **α-PAC-2-PF_6/CF_3SO_3 (x = @)** (red, x = 1; blue, x = 0.75; green, x = 0.50; purple, x = 0.25; black, x = 0).

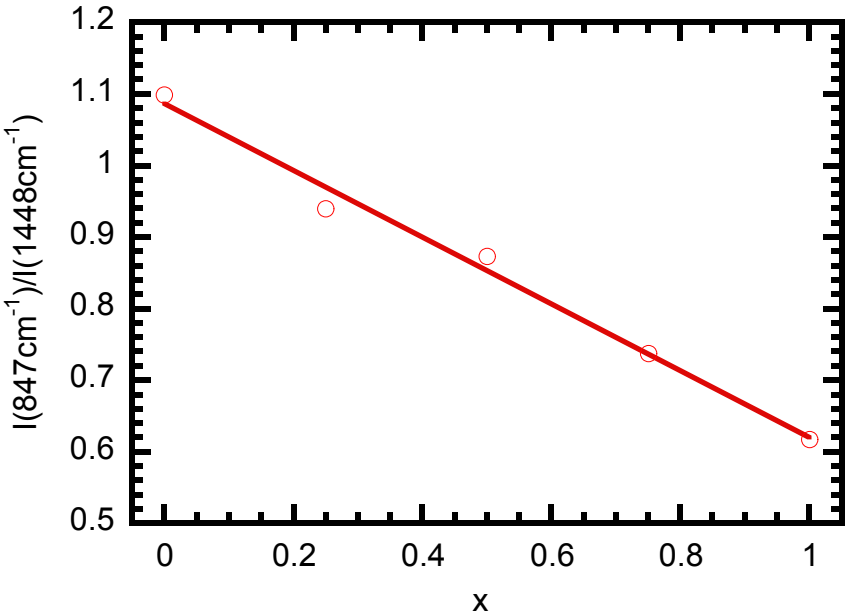

Fig. S2. Plot of x vs I(847cm^{-1})/I(1448cm^{-1}), where I(847cm^{-1}) and I(1448cm^{-1}) are intensities at each wavenumber. The bands at 847 and 1448 cm^{-1} are assigned as a PF_6^- ν_3 vibration and a pyridine ring stretching vibration, respectively.[1,2] The solid line represents the least-squares liner fit.

2. TG analysis

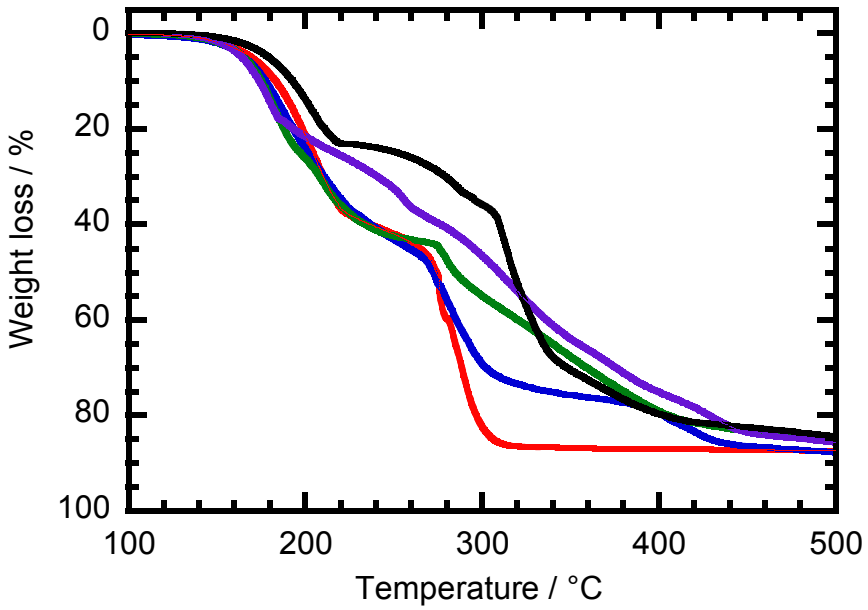

Fig. S3. TG curves of **α-PAC-2-PF_6/CF_3SO_3 (x = @)** (red, x = 1; blue, x = 0.75; green, x = 0.50; purple, x = 0.25; black, x = 0).

3. UV-vis spectra

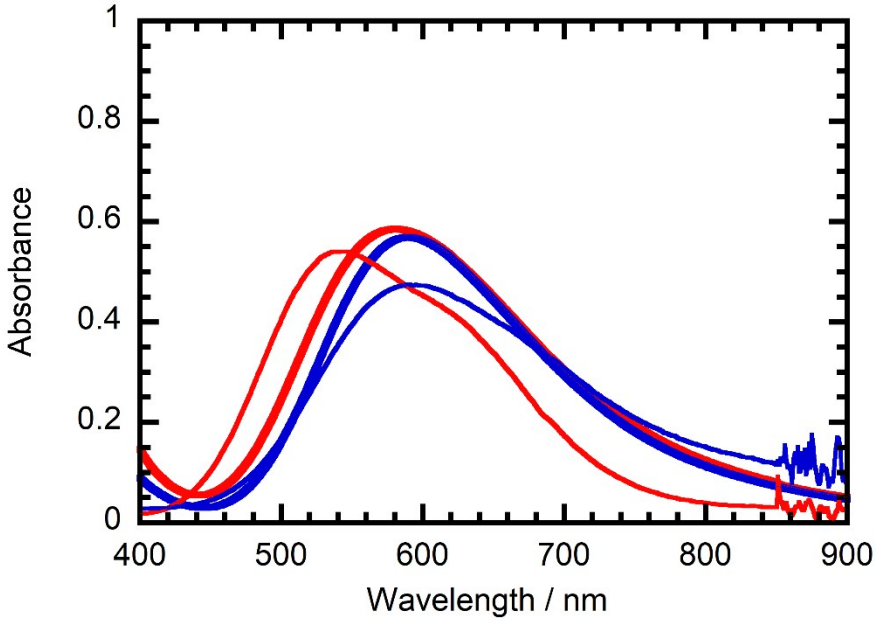

Fig. S4. UV-vis spectra of **α-PAC-2-PF_6** (red) and **α-PAC-2-CF_3SO_3** (blue) in acetone solution (thick lines) and solid state (thin lines).

4. Powder X-ray diffraction patterns

Table S1. Unit cell parameters for **α-PAC-2-PF_6/CF_3SO_3 (x = @)** derived from Pawley fitting.

x	*a* / Å	*b* / Å	*c* / Å	*β* / °	*V* / Å^3	R_p / %	R_{wp} / %
0	10.546(2)	16.272(3)	16.851(3)	-	2892(1)	5.13	7.48
0.25	10.553(5)	16.253(5)	16.818(8)	-	2885(2)	8.66	12.45
0.25	10.57(1)	14.81(2)	18.30(2)	92.17(5)	2864(5)	8.18	12.62
0.5	10.462(5)	14.473(6)	18.213(8)	91.57(2)	2757(2)	3.00	4.07
0.75	10.482(5)	14.436(6)	17.953(6)	91.94(2)	2715(2)	3.14	4.31
1	10.434(6)	14.323(7)	17.622(8)	92.03(2)	2632(2)	3.72	5.43

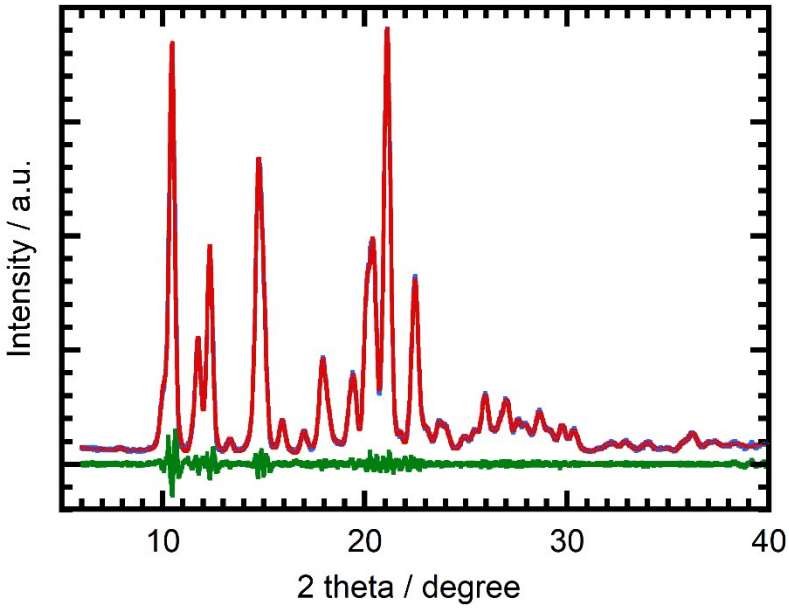

Fig. S5. Pawley fit of the PXRD pattern of **α-PAC-2-PF_6/CF_3SO_3 (x = 1)**. The blue, red, and green lines represent the experimental, calculated and difference profile, respectively. The space group was determined to be $P2_1/c$ by the indexing routine of the TOPAS program package.

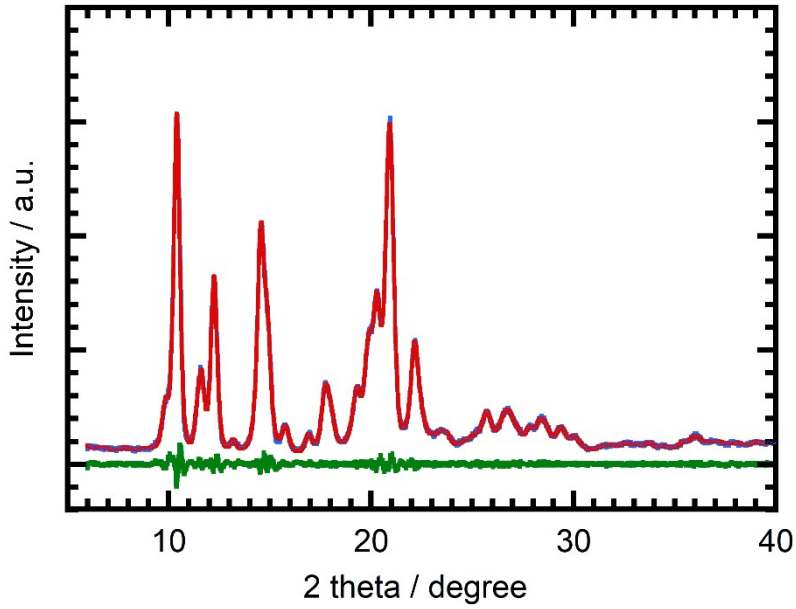

Fig. S6. Pawley fit of the PXRD pattern of **α-PAC-2-PF_6/CF_3SO_3 (x = 0.75)**. The blue, red, and green lines represent the experimental, calculated and difference profile, respectively. The space group was determined to be $P2_1/c$ by the indexing routine of the TOPAS program package.

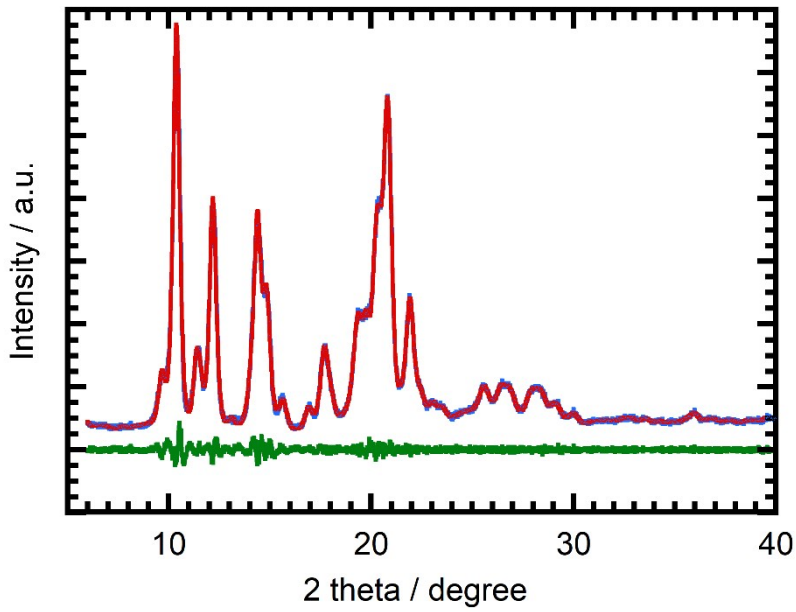

Fig. S7. Pawley fit of the PXRD pattern of **α-PAC-2-PF_6/CF_3SO_3 (x = 0.5)**. The blue, red, and green lines represent the experimental, calculated and difference profile, respectively. The space group was determined to be $P2_1/c$ by the indexing routine of the TOPAS program package.

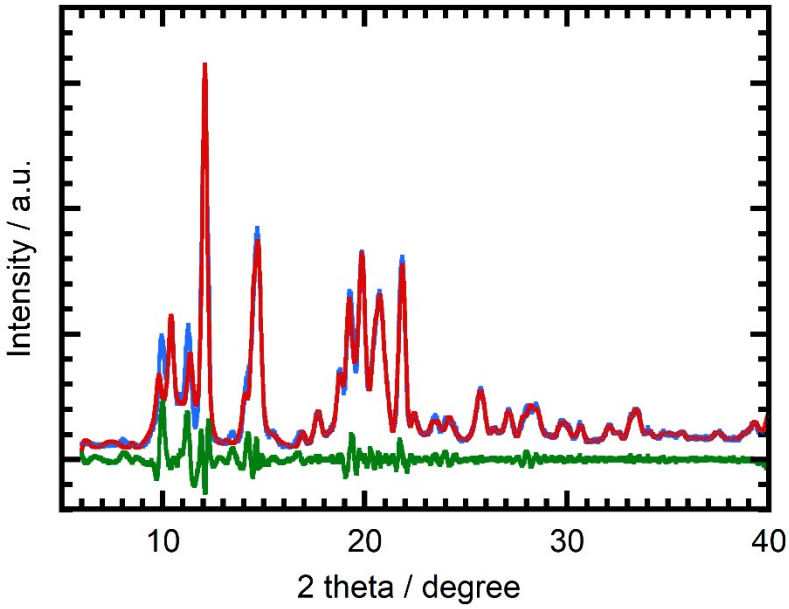

Fig. S8. Pawley fit of the PXRD pattern of **α-PAC-2-PF_6/CF_3SO_3 (x = 0.25)**. The blue, red, and green lines represent the experimental, calculated and difference profile, respectively. The space group was determined to be $P2_1/c$ by the indexing routine of the TOPAS program package.

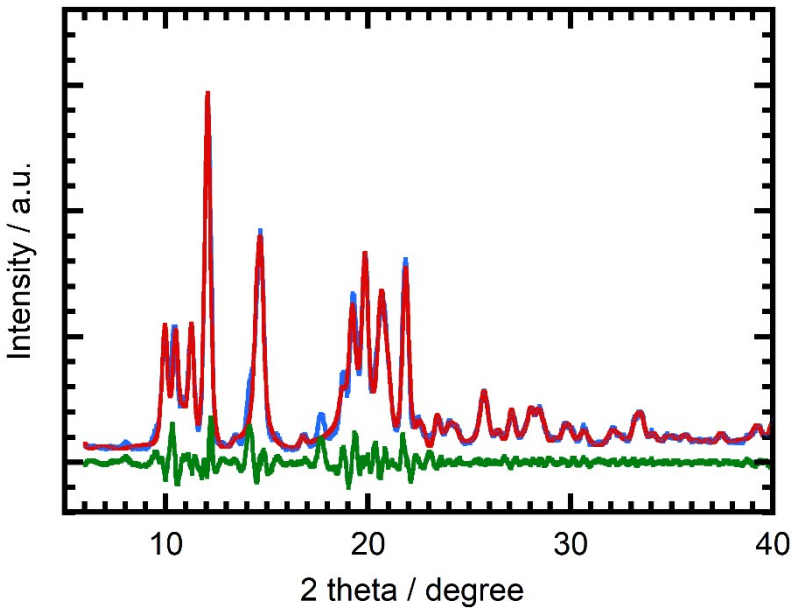

Fig. S9. Pawley fit of the PXRD pattern of **α-PAC-2-PF_6/CF_3SO_3 (x = 0.25)**. The blue, red, and green lines represent the experimental, calculated and difference profile, respectively. The space group was determined to be *Pbcn* by the indexing routine of the TOPAS program package.

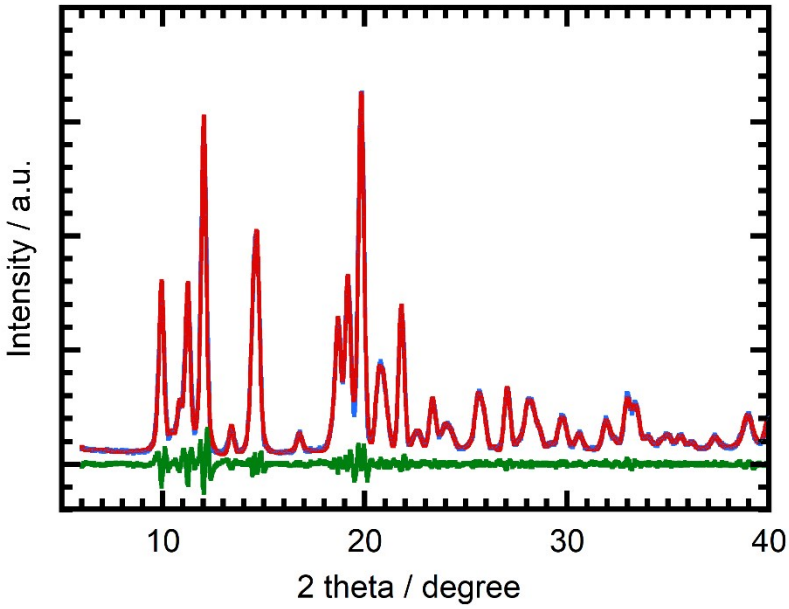

Fig. S10. Pawley fit of the PXRD pattern of **α-PAC-2-PF_6/CF_3SO_3 (x = 0)**. The blue, red, and green lines represent the experimental, calculated and difference profile, respectively. The space group was determined to be *Pbcn* by the indexing routine of the TOPAS program package.

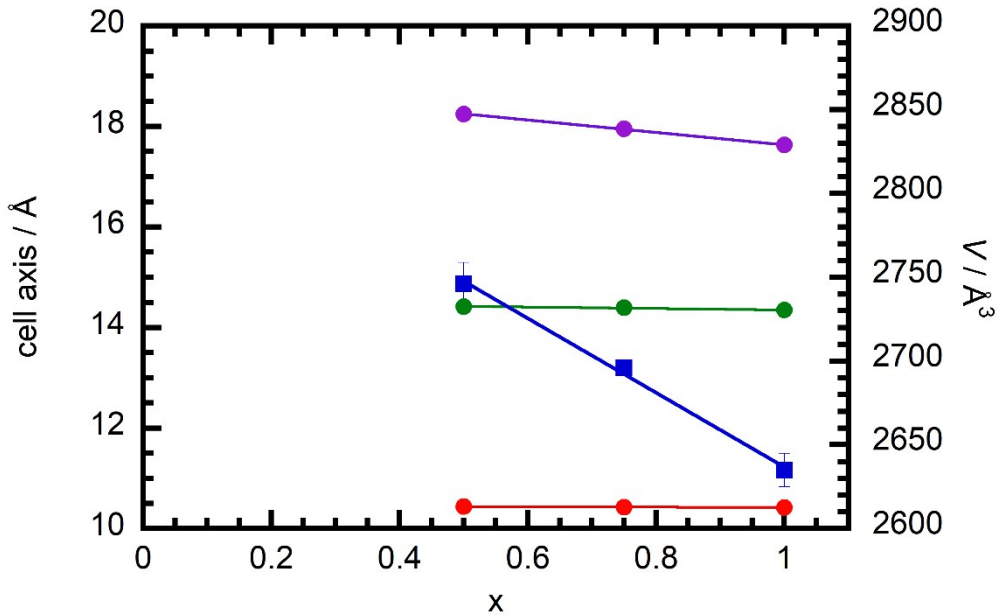

Fig. S11. Composition ratio-dependent cell parameters of **α-PAC-2-PF_6/CF_3SO_3 (x = @)**. Red, green, purple, and blue symbols indicate *a*, *b*, *c*, and *V*, respectively.

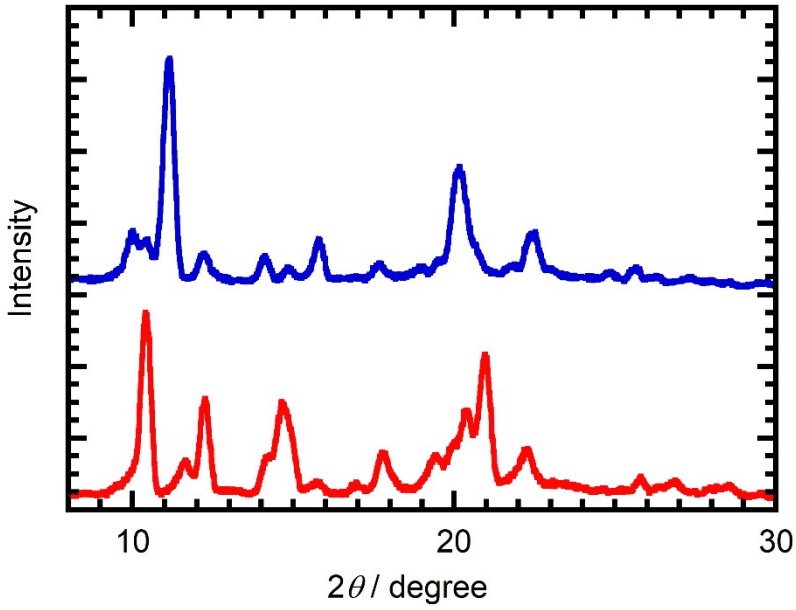

Fig. S12. PXRD patterns of **α-PAC-2-PF_6/CF_3SO_3(x = 0.75)** before (red) and after (blue) an exposure to a saturated acetone vapor.

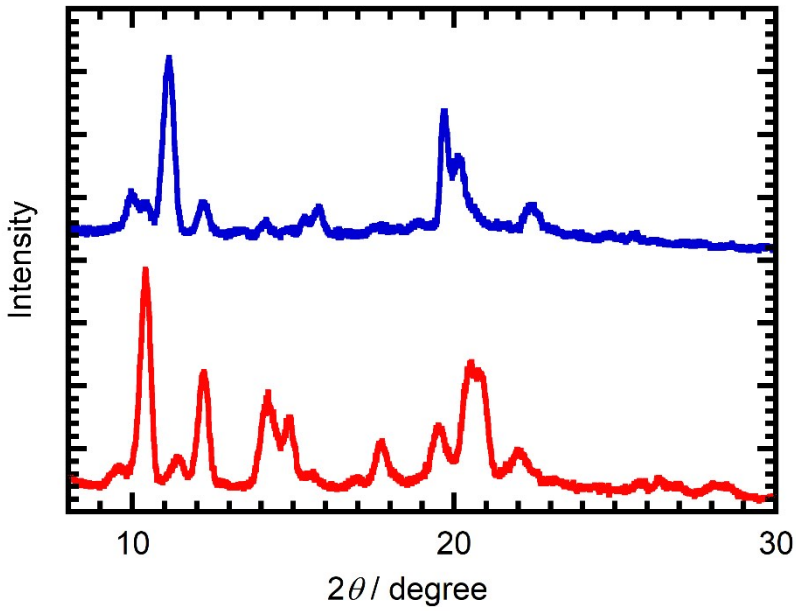

Fig. S13. PXRD patterns of **α-PAC-2-PF_6/CF_3SO_3(x = 0.5)** before (red) and after (blue) an exposure to a saturated acetone vapor.

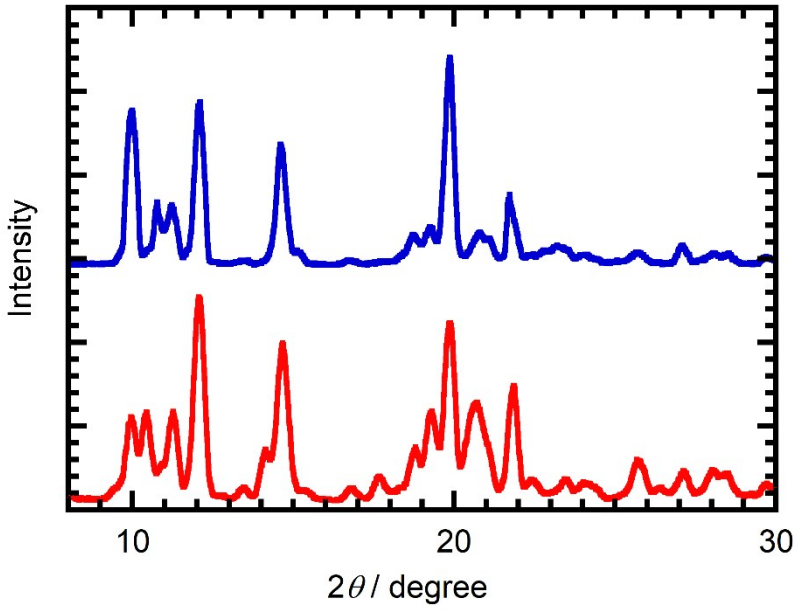

Fig. S14. PXRD patterns of **α-PAC-2-PF_6/CF_3SO_3(x = 0.25)** before (red) and after (blue) an exposure to a saturated acetone vapor.

5. Acetone sorption properties

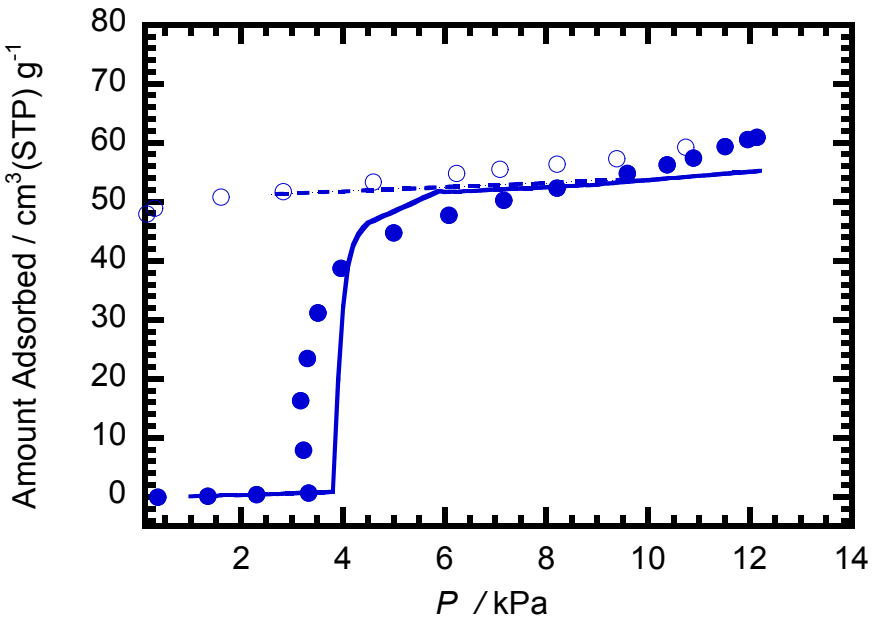

Fig. S15. Acetone adsorption/desorption isotherms (adsorption, closed symbols; desorption, open symbols) in **α-PAC-2-PF_6/CF_3SO_3 (x = 0.75)** at 288 K. The solid and dashed lines indicate the adsorption/desorption isotherms of physical mixture (**α-PAC-2-PF_6** : **α-PAC-2-CF_3SO_3** = 0.75 : 0.25) calculated using the acetone adsorption/desorption data of pure **α-PAC-2-PF_6** and **α-PAC-2-CF_3SO_3**.

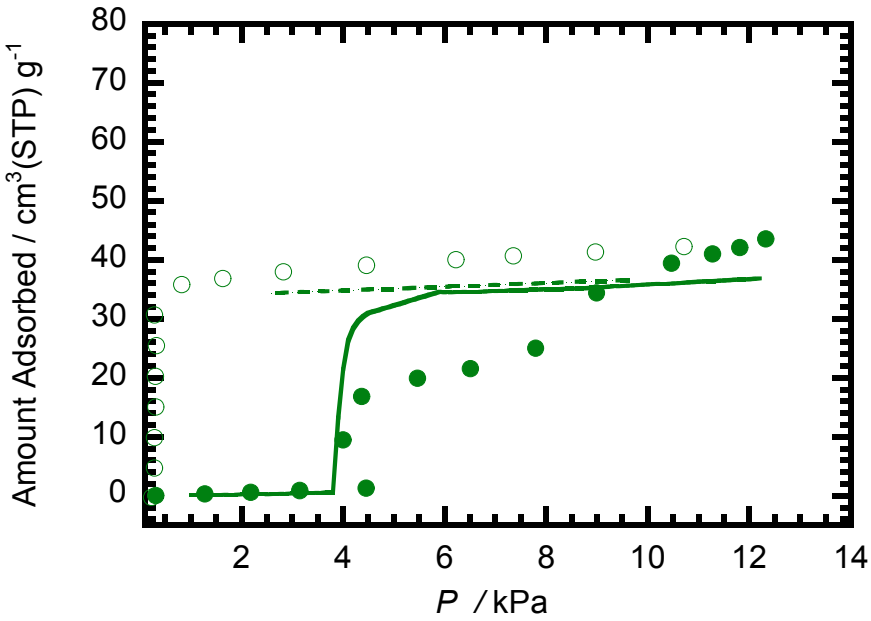

Fig. S16. Acetone adsorption/desorption isotherms (adsorption, closed symbols; desorption, open symbols) in **α-PAC-2-PF_6/CF_3SO_3 (x = 0.5)** at 288 K. The solid and dashed lines indicate the adsorption/desorption isotherms of physical mixture (**α-PAC-2-PF_6** : **α-PAC-2-CF_3SO_3** = 0.5 : 0.5) calculated using the acetone adsorption/desorption data of pure **α-PAC-2-PF_6** and **α-PAC-2-CF_3SO_3**.

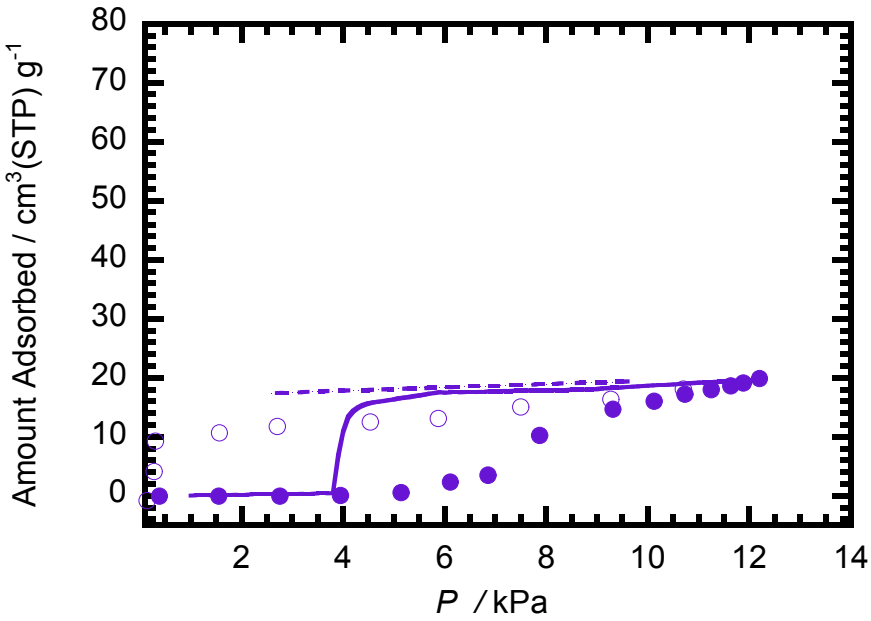

Fig. S17. Acetone adsorption/desorption isotherms (adsorption, closed symbols; desorption, open symbols) in **α-PAC-2-PF_6/CF_3SO_3 (x = 0.25)** at 288 K. The solid and dashed lines indicate the adsorption/desorption isotherms of physical mixture (**α-PAC-2-PF_6** : **α-PAC-2-CF_3SO_3** = 0.25 : 0.75) calculated using the acetone adsorption/desorption data of pure **α-PAC-2-PF_6** and **α-PAC-2-CF_3SO_3**.

6. Theoretical calculations

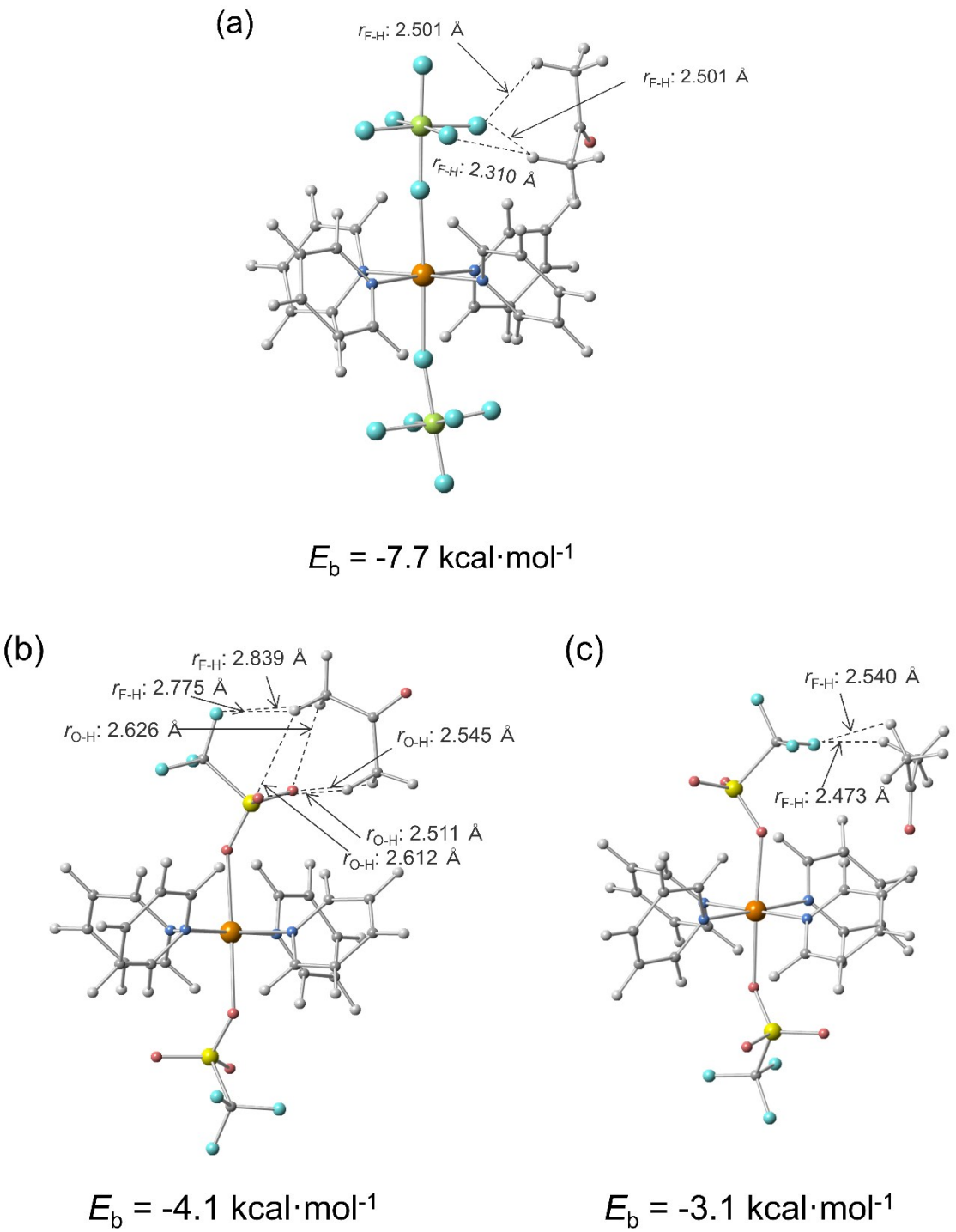

Fig. S18. Optimized structures of (a) {[$Cu(PF_6)_2(py)_4$]·acetone}, (b) {[$Cu(CF_3SO_3)_2(py)_4$]·acetone} with the interaction between acetone and F/O atoms of CF_3SO_3 anion, and (c) {[$Cu(CF_3SO_3)_2(py)_4$]·acetone} with the interaction between

acetone and F atom of CF_3SO_3. The binding energy of acetone for $[Cu(PF_6)_2(py)_4]$ was larger than those for $[Cu(CF_3SO_3)_2(py)_4]$.

7. References

1. S. Noro, R. Matsuda, Y. Hijikata, Y. Inubushi, S. Takeda, S. Kitagawa, Y. Takahashi, M. Yoshitake, K. Kubo and T. Nakamura, High CO_2/CH_4 Selectivity of a Flexible Copper(II) Porous Coordination Polymer under Humid Conditions. *ChemPlusChem*, 2015, **80**, 1517.
2. R. M. Silverstein, F. X. Webster, D. J. Kiemle and D. L. Bryce, *Spectrometric Identification of Organic Compounds*, eighth ed.; Wiley, 2014.